nature photonics

Article

https://doi.org/10.1038/s41566-026-01845-y

Efficient integrated quantum memory for light

Received: 10 February 2025

Accepted: 8 January 2026

Published online: 11 February 2026

Check for updates

Ruo-Ran Meng[1,2,3,5], Pei-Xi Liu[1,2,3,5], Xiao Liu[1,2,3,5], Tian-Xiang Zhu[1,2,3,5], Peng-Jun Liang[1,2,3,4,5], Chao Zhang[1,2,3,4,5], Zhong-Yang Tang[1,2,3], Hong-Zhe Zhang[1,2,3], Jin-Ming Cui[1,2,3,4], Ming Jin[1,2,3] ✉, Zong-Quan Zhou[1,2,3,4] ✉, Chuan-Feng Li[1,2,3,4] ✉ & Guang-Can Guo[1,2,3,4]

Scalable implementation of quantum networks and photonic processors demands integrated photonic memories with high efficiency, yet current integrated systems have been limited to storage efficiencies below 27.8%. Here we demonstrate highly efficient integrated quantum memories based on rare-earth-ion-doped crystals coupled with impedance-matched microcavities, realized in two novel architectures: 200-μm-thin membranes of Eu^{3+}:Y_2SiO_5 integrated with fibre-based microcavities and waveguide-based cavities fabricated using femtosecond lasers. Our approach achieves reliable integrated quantum storage with record efficiencies of 80.3(7)% for weak coherent pulses and 69.8(1.6)% for telecom-heralded single photons, alongside the storage of 20 temporal modes with an average efficiency of 51.3(2)%. Moreover, the thin-membrane Eu^{3+}:Y_2SiO_5 architecture enables spectrally tunable efficient quantum storage via variable strain, providing a flexible interface for quantum networks. By combining high efficiency, large multimode capacity and tunability, our devices establish a versatile hardware foundation for scalable quantum repeaters and chip-scale photonic processors.

Optical quantum memory, capable of storing and retrieving quantum states of light, is a foundational technology for long-distance quantum networks[1–3] and for photonic information processing[4–6]. Storage efficiency is a key figure of merit[1,7] because higher efficiency can boost the rate of entanglement distribution in quantum repeaters[1] and improves the success probabilities of multiphoton generation and quantum gate operations in optical quantum computing[4–6]. A pivotal efficiency threshold is 50%, which is the necessary condition to operate in the no-cloning regime without postselection[8] and for implementing error correction protocols in one-way quantum computation[9].

Quantum storage of light leverages collective enhancement in atomic ensembles, whether gaseous or solid-state[10–15], or strong coupling of single atoms with optical cavities[16,17]. So far, the highest reported quantum storage efficiency has reached 90.6% in cold atomic gases using the electromagnetically induced transparency scheme[11,18], 82% in warm atomic vapours via Raman memory[19] and 69% in rare-earth-ion (REI)-doped solids employing the gradient echo memory scheme[14], all operating on microsecond timescales. However, these approaches require physically large medium ($\sim 10^{-1}$–10^{4} mm^3) and are limited to single temporal modes because the underlying memory protocols suffer from inherently low multimode capacity[20]. Integrated quantum memories for light have been demonstrated in REI-doped solids[7,21–25], successfully reducing the medium size by several orders of magnitude (Fig. 5), but the

[1]Laboratory of Quantum Information, University of Science and Technology of China, Hefei, China. [2]Anhui Province Key Laboratory of Quantum Network, University of Science and Technology of China, Hefei, China. [3]CAS Center For Excellence in Quantum Information and Quantum Physics, University of Science and Technology of China, Hefei, China. [4]Hefei National Laboratory, University of Science and Technology of China, Hefei, China. [5]These authors contributed equally: Ruo-Ran Meng, Pei-Xi Liu, Xiao Liu, Tian-Xiang Zhu, Peng-Jun Liang, Chao Zhang. ✉e-mail: cattom@ustc.edu.cn; zq_zhou@ustc.edu.cn; cfli@ustc.edu.cn

https://doi.org/10.1038/s41566-026-01845-y

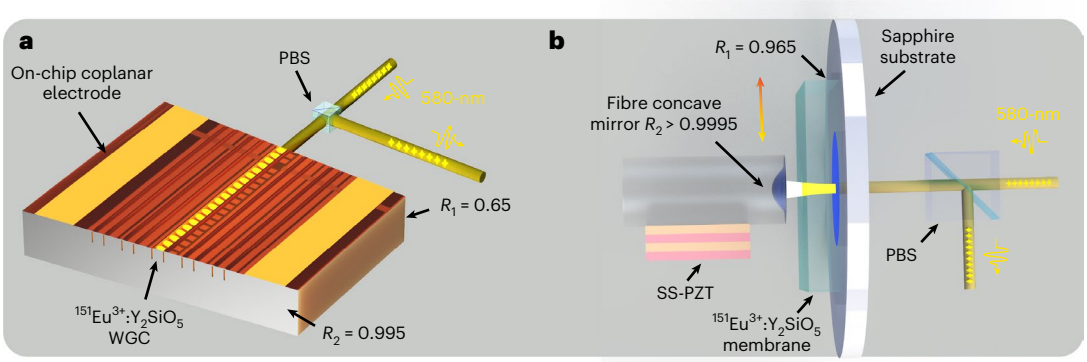

Fig. 1 | The devices for efficient integrated quantum memories based on REI doped crystals. a, Efficient quantum memories based on the WGC fabricated on $^{151}Eu^{3+}$:Y_2SiO_5 crystals. Laser-written optical waveguides are coated with reflective layers at both ends to form optical cavities. On-chip coplanar electrodes deliver electrical pulses, enabling active control over the readout times of stored photons. Input and readout photons are separated by a polarizing beam splitter (PBS) depending on their different polarization states, with multiplexing achieved in the time domain. **b**, Efficient quantum memories based on the FBC. This cavity consists of a fibre concave mirror and a 200-μm-thin membrane $^{151}Eu^{3+}$:Y_2SiO_5 crystals with reflective coatings on its outer surface. The membrane is bonded to a sapphire substrate with a hole. The concave fibre mirror fixed on the stacked shearing piezoelectric transducer (SS-PZT) maintains a distance of approximately 100 μm from the membrane surface. The input and output signal photons are also separated using a PBS.

highest storage efficiency achieved so far remains limited to 27.8%[23], presenting a substantial hurdle for their practical deployment in quantum networks.

In this work, we introduce highly efficient integrated quantum memories based on $^{151}Eu^{3+}$:Y_2SiO_5 crystals coupled with impedance-matched optical cavities. Two novel microcavity configurations are utilized for the quantum storage of light: the waveguide cavity (WGC) and the fibre-based microcavity (FBC), as shown in Fig. 1. The WGC is constructed by applying reflective coatings to the end surfaces of an on-chip laser-written optical waveguide, incorporating coplanar electrodes for on-demand retrieval via electric pulse control[23]. This configuration achieves a storage efficiency of 80.3(7)% for single-photon-level weak coherent inputs, the highest efficiency reported for photonic storage in solid-state systems. The FBC employed hundred-micron $^{151}Eu^{3+}$:Y_2SiO_5 membranes integrated into a FBC, achieving a storage efficiency of 69.8(1.6)% for telecom-heralded single photons. It successfully stores 20 temporal modes with an average efficiency exceeding 50%. In addition, by applying strain to the membranes, the optical absorption centre is tuned over a 10 GHz range, enabling efficient quantum storage with adjustable centre frequencies. Although microcavities have previously been exploited to address individual REIs in the Purcell regime[26–28], our FBC operates in a distinct regime that harnesses the collective coupling of a REI ensemble with light.

Results

Theoretical description

Efficient storage of light intuitively demands a medium with strong optical absorption. However, the coherent intra-4*f* optical transitions of REI are generally weak due to the parity-forbidden nature of the electric dipole transition. This challenge is particularly prominent for the $^7F_0 \rightarrow {}^5D_0$ optical transition of the Eu^{3+}:Y_2SiO_5 crystal, a promising candidate for long-lived quantum memory that has enabled coherent light storage for 1 h (refs. 29,30). Preliminary approaches have been explored to achieve efficient integrated quantum memories, such as increasing the interaction length with long bent or spiral on-chip waveguides or integrating quantum memories with photon sources in a single cavity[31]; however, these approaches have yet to reach high efficiency and remain technologically demanding. A broadly applicable solution to address the weak absorption issue is to introduce an impedance-matched optical cavity, which enables near-unity storage efficiency even with optically thin medium[32–34]. The impedance-matched condition is given by $R_1 = e^{-2\tilde{d}}$ and $R_2 = 1$, where R_1 and R_2 are the reflectivities of the coupling and second mirrors, respectively, and $\tilde{d}$ is the effective absorption depth averaged over the input bandwidth. Under this condition, assuming $\epsilon \ll \tilde{d} \ll 1$, the storage efficiency of a cavity-enhanced quantum memory simplifies to[33,34]

$$\eta = \frac{\eta_M \times \eta_{deph}}{\left(1 + \frac{\epsilon}{4\tilde{d}}\right)^4}, \quad (1)$$

where ϵ is the optical depth of round-trip intracavity loss, η_M is the mode-matching efficiency between the input light and the cavity mode and η_{deph} accounts for the remaining atomic dephasing. Achieving efficiencies close to 100% requires $\eta_M, \eta_{deph} \approx 1$ and $\epsilon/4\tilde{d} \ll 1$.

This impedance-matched cavity approach has been implemented with bulk REI-doped crystals using the atomic frequency comb (AFC) protocol[35–37], whose absorption profile consists of a series of periodic peaks. To date, however, the efficiencies achieved remain below that of single-pass long-crystal configurations[14]. Here, we present two compact cavity designs that simultaneously deliver high η_M and low ϵ, enabling efficient integrated quantum storage. For cavity-enhanced AFC memories, achieving $\eta_{deph} \approx 1$ requires a high finesse of the AFC structure(F_{AFC}), which places stringent demands on the peak absorption depth d, as $F_{AFC} \approx d/\tilde{d}$ (ref. 36). However, creating an AFC with strong absorption often induces a slow-light effect[37,38], which limits the achievable bandwidth and hinders temporal multimode storage. To solve this dilemma, we employ an absorption-enhanced spectral hole-burning technique to prepare AFC with enhanced absorption embedded within a transparency pit, so that the fast-light dispersion caused by the enhanced AFC could counteract the slow-light dispersion caused by the spectral pit (see Supplementary Section 8 for details). This approach enables the preparation of high-finesse AFC while suppressing slow-light effects, thereby preserving a relatively large system bandwidth and facilitating efficient storage of multiple temporal modes.

Memory performance

Gaussian-shaped weak coherent pulses with a full width at half maximum (FWHM) of 0.45 μs and 0.19 μs are used for the WGC and FBC, respectively, with average photon numbers per pulse (μ) of 0.35 and 0.70. As shown in Figs. 2a and 3a, single pulses are stored and retrieved for 1 μs for the WGC and 2 μs for the FBC, achieving efficiencies of 80.3(7)% and 75.2(5)%, respectively. Although FBC exhibits a lower $\epsilon/4\tilde{d}$ than WGC, the WGC achieves a higher storage efficiency due to its

https://doi.org/10.1038/s41566-026-01845-y

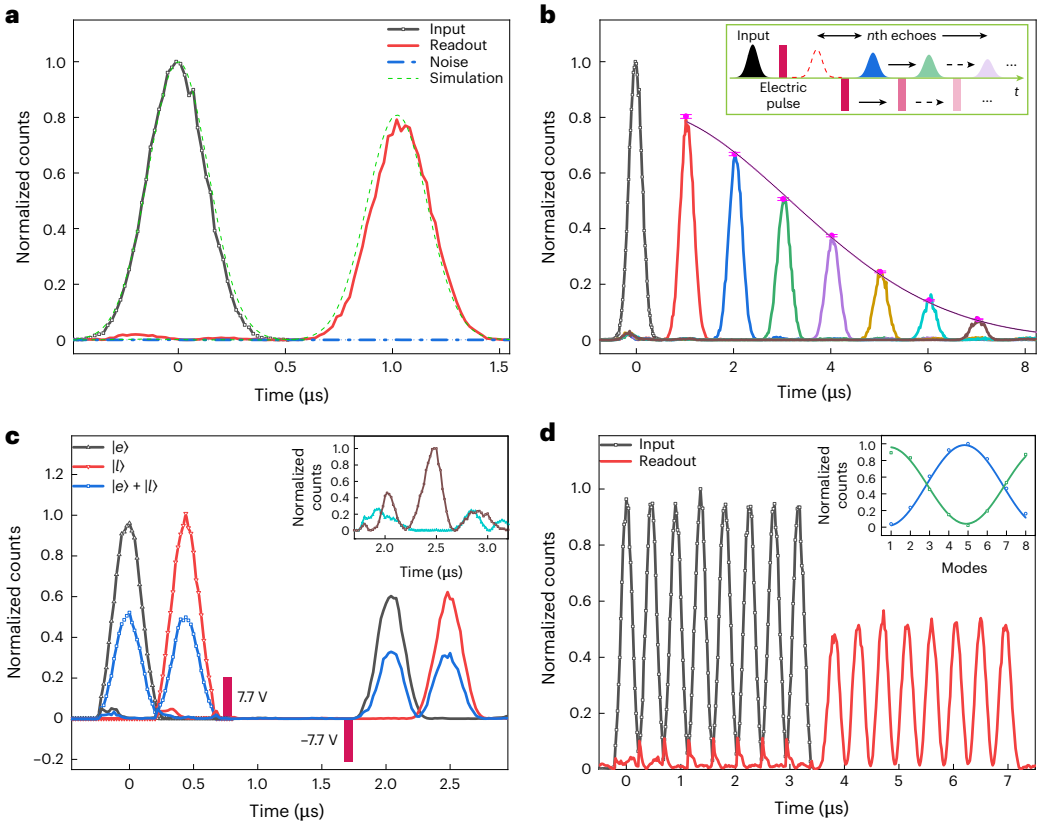

Fig. 2 | Efficient and multiplexed single-photon-level storage in the WGC. **a**, Normalized photon-counting histograms for the first AFC echo. The red solid line represents the first AFC echo, compared with the reference input signal (black solid line with hollow squares) at an average photon number per pulse $\mu = 0.35$. Noise measurements with zero input are shown as a blue dot-dashed line. The storage efficiency of the first AFC echo is 80.3(7)%, while the simulation (green dashed line) predicts a slightly higher efficiency of 80.9%. **b**, Photon-counting histograms of higher-order AFC echoes with $\mu = 0.35$. Inset: the on-demand storage sequence over time (t), where two electric pulses actively control the readout times through Stark-shift induced interference. The fitted efficiency decay (pink solid line) yields an AFC finesse of F_{AFC} of 11.9(1), consistent with the expected value for the impedance-matched condition. **c**, On-demand storage of time-bin qubits. Three input states $|e\rangle$, $|l\rangle$, and $|e\rangle + |l\rangle$ are presented in the histogram. The average photon number per qubit $\mu_q = 0.35$, with an average storage efficiency of 62.0(6)%. Inset: interference measurements on the superposition state $|e\rangle + |l\rangle$, with constructive (brown solid line with hollow squares) and destructive interference (cyan solid line with hollow triangles). **d**, Storage of eight temporal modes with an average efficiency of 52.9(2)%. The FWHM of the temporal modes is set as 0.23 μs with each mode containing $\mu = 0.17$. Inset: the interference between the retrieved multimode echoes and reference pulses with two initial phases differing by π, yielding an average visibility of 0.94(4).

higher η_M and η_{deph}, as summarized in Table 1. The quantum storage efficiency of WGC surpasses both the highest quantum storage efficiency (69%)[14] and the highest light storage efficiency (76%)[39] achieved in any solid-state medium. The theoretical efficiency of the WGC is estimated to be 81.5% according to equation (1), and the simulated efficiency based on measured cavity parameters is 80.9% (Fig. 2a). Both numbers align well with our experimental results. Details about the simulation of the storage process are provided in the Supplementary Section 8. Reducing ϵ from 0.029 to 0.01 in the WGC could enable storage efficiency of above 90%.

We demonstrate on-demand retrieval of input photons in the WGC using Stark-shift-induced interference for active control of readout times[23,40]. After the absorption of input photons, two electric pulses (FWHM of 48 ns, voltage of ±7.7 V) are applied to read out the photons in an arbitrary order of AFC echoes. Figure 2b shows the first to seventh AFC echoes with $\mu = 0.35$, where efficiency decay follows a Gaussian profile, yielding a fitted F_{AFC} of 11.9(1), consistent with the expected value for the impedance-matched condition.

To benchmark the quantum storage fidelity, time-bin qubits are encoded onto input photons. Photon-counting histogram for qubit states $|e\rangle$, $|l\rangle$ and $|e\rangle+|l\rangle$ are shown in Figs. 2c and 3b, where $|e\rangle$ and $|l\rangle$ represent the early and the late qubit states, respectively. The fidelities of the superposition states ($|e\rangle + |l\rangle$ and $|e\rangle + i|l\rangle$) are analysed using an independent AFC-based analyser for the FBC[37] and a double-AFC structure for the WGC[23] (see Supplementary Section 7 for details). The measured fidelities, summarized in Supplementary Table 3, reveal a minimum total fidelity of 99.0(1)%, which indicates a strong violation of the fidelity bound that can be achieved with the classical measure-and-prepare strategy[16,23], confirming that the memories are unambiguously operating in the quantum regime. We note that the large bandwidth achieved in the FBC ensures that the storage efficiency for time-bin qubits (74.6(6)%) closely matches that for single pulses (75.2(5)%).

In the FBC configuration, we extend the storage time to 10 μs and demonstrate the storage of 20 temporal modes with an average storage efficiency of 51.3(2)% (Fig. 3c). For the WGC, eight temporal modes are stored with an average storage efficiency of 52.9(2)% over a storage time of 3.8 μs (Fig. 2d). The reduced temporal multimode capacity of the WGC is attributed to a narrower storage bandwidth and a shorter two-level AFC lifetime. The former is constrained by the cavity linewidth due to a stronger slow-light effect, whereas the latter is limited by a shorter optical coherence lifetime (measured with two-pulse photon echoes), most likely induced by stronger vibrations in the WGC cryostat.

To confirm coherence preservation in the retrieved multimode echoes, we measure the interference fringes between retrieved echoes

https://doi.org/10.1038/s41566-026-01845-y

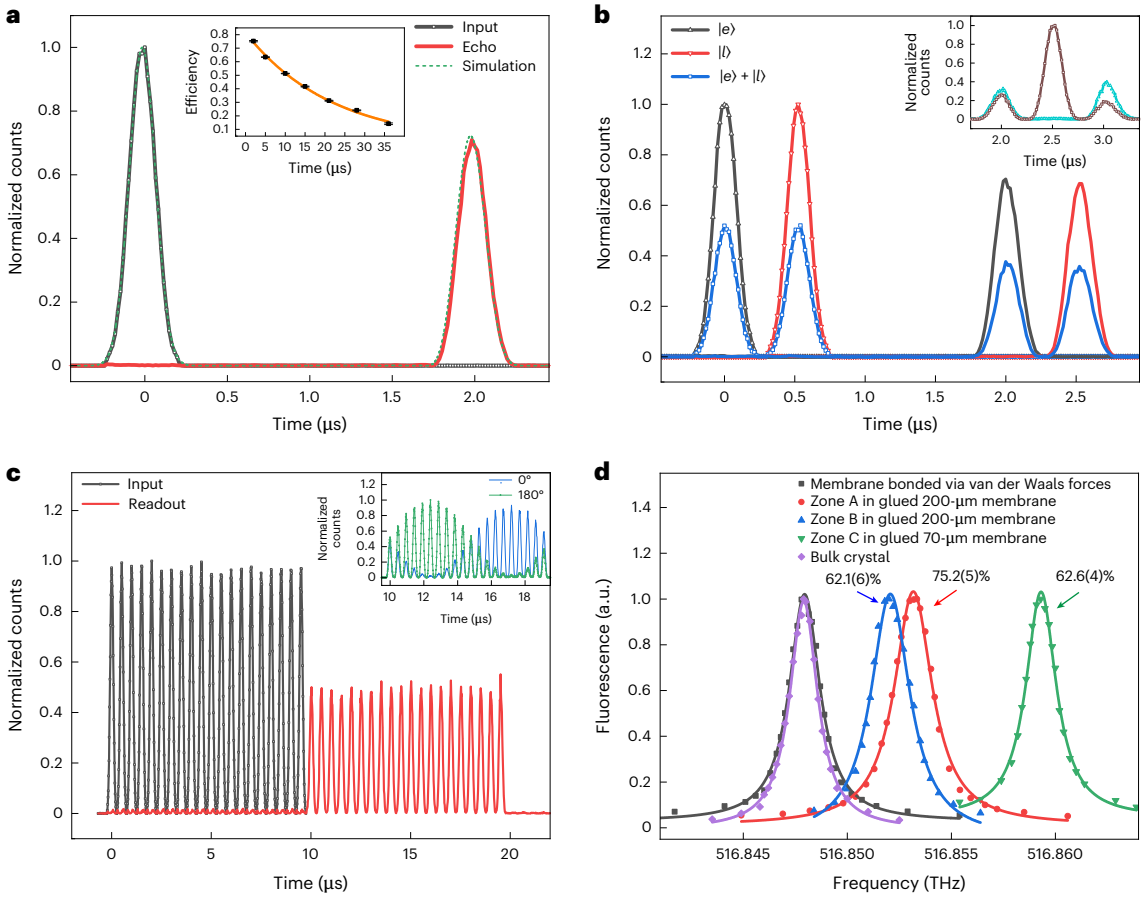

Fig. 3 | Efficient and spectrally tunable quantum storage using $^{151}Eu^{3+}$:Y_2SiO_5 membranes coupled into the FBC. a, Photon-counting histograms of storage for weak coherent pulses with $\mu = 0.35$, with an efficiency of 75.2(5)% at 2 μs, while the simulation (green dashed line) predicts a slightly higher efficiency of 78.4%. Inset: efficiency decay fitted with an exponential decay function $\exp(-4t/T_{AFC}^{eff})$, yielding an effective AFC lifetime $T_{AFC}^{eff} = 87.6(2.4)\,\mu s$. **b**, Storage of time-bin qubits with an average photon number per qubit $\mu_q = 0.7$. Inset: the interference measurements for the superposition state $|e\rangle + |l\rangle$. **c**, Quantum storage of 20 temporal modes with average efficiency of 51.3(2)% at $\mu = 0.7$. Inset: the interference between retrieved multimode echoes and reference pulses, yielding an average visibility of 0.94(1). **d**, Photoluminescence excitation spectra of $^{151}Eu^{3+}$:Y_2SiO_5 membranes under variable strain. Lorentz fits reveal fluorescence centres at 516.8479 THz (black), 516.8479 THz (purple), 516.8521 THz (blue), 516.8532 THz (red) and 516.8593 THz (green). Quantum storage efficiencies achieved at the latter three frequencies are 62.1(6)%, 75.2(5)% and 61.6(4)%, respectively.

Table 1 | The device parameters for FBC and WGC

System	η_M	F_{AFC}	η_{deph}	$\epsilon/4\tilde{d}$	$(1+\epsilon/4\tilde{d})^{-4}$	η_{Theo}	η_{Exp}
FBC	95%	8	89.6%	1/40	90.6%	77.1%	75.2(5)%
WGC	98.5%	12	95.2%	1/28	86.9%	81.5%	80.3(7)%

η_{Theo}, theoretical storage efficiency derived from equation (1); η_{Exp}, the experimentally measured storage efficiency.

and reference pulses (see Supplementary Section 7 for details). Given the multiple temporal modes, we observe a complete sine oscillation fringe by linearly varying the phase of all input modes while maintaining the reference pulse phase constant (Figs. 2d and 3c, inset). The measured interference visibilities of 0.94(4) for the WGC and 0.94(1) for the FBC confirm reliable quantum storage of multiple temporal modes.

In the FBC configuration, the membrane flat mirror is bonded to a sapphire substrate with a central hole using epoxy resin adhesive. This bonding process introduces variable strain to the membrane as the adhesive solidifies and cools, shifting the optical absorption centre frequency of $^{151}Eu^{3+}$ ions via the piezospectroscopic effect[41]. As shown in Fig. 3d, we measure the photoluminescence spectra of membranes. For the aforementioned 200 μm membrane with a storage efficiency of 75.2(5)%, the absorption centre frequency is observed at 516.8532 THz. At a different location on the same membrane, the absorption centre frequency shifts to 516.8521 THz, where a quantum storage efficiency of 62.1(6)% is measured for weak coherent pulses. Furthermore, a thinner membrane with a thickness of 70 μm shows an absorption centre frequency of 516.8593 THz, with a measured storage efficiency of 61.6(4)%. These variations in efficiency are attributed to increased intracavity loss, probably caused by dust on the fibre concave mirror during membrane switching. Notably, membranes attached to fused quartz substrates via van der Waals forces exhibit an absorption centre frequency of 516.8479 THz, nearly identical to that of bulk crystals without additional strain. An optical frequency shift of 10 GHz implies a pressure of ~47 MPa in Eu^{3+}:Y_2SiO_5 crystals[42]. This notable pressure probably originates from shear strain generated in the thin membranes. Although strain in bulk crystals typically induces both frequency shifts and additional broadening[41], strain in hundred-micron membranes can cause substantial optical frequency shifts (~10 GHz) with negligible broadening, thus preserving the original absorption depth for efficient quantum storage. This property enables the realization of spectrally tunable and efficient quantum memories, which could facilitate wideband spectral multiplexing[24,25] within a single device through controlled strain, and flexible interfacing with quantum light sources based on free atoms, where achieving large spectral tuning on the atomic side poses substantial challenges.

https://doi.org/10.1038/s41566-026-01845-y

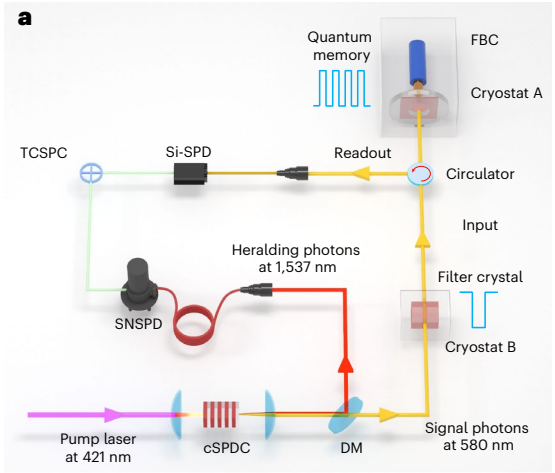

Fig. 4 | Efficient storage of telecom-heralded single photons in the FBC. **a**, A 421-nm laser pumps a nonlinear crystal, generating photon pairs at 1,537 and 580 nm via cavity-enhanced spontaneous parametric down-conversion (cSPDC). Photon pairs are separated by a dichroic mirror (DM). The 1,537-nm telecom-band photons are detected by a superconducting nanowire single-photon detector (SNSPD), providing heralding signals. The 580-nm signal photons are spectrally filtered using an optically pumped filter crystal, resulting in a bandwidth of 4 MHz. After storage in the FBC quantum memory, the readout photons are extracted by an optical circulator and detected by a silicon-based single-photon detector (Si-SPD). Coincidence measurements of the photon pairs are performed using a time-correlated single-photon-counting (TCSPC) module. **b**, Photon-counting histograms for storage of heralded single photons. The measured storage efficiency is 69.8(1.6)% at 2 μs with a cross-correlation of 16.4(2) within a 123-ns window, confirming non-classical correlations between retrieved photons and telecom heralding photons.

Storage of single photons

All previous demonstrations of efficient solid-state quantum memories[14,37] are implemented with attenuated laser pulses rather than true quantum light, despite the latter being essential for practical quantum network applications such as quantum repeaters[1,3,43] or photonic quantum computing[4–6]. So far, the maximum storage efficiency for single photons in solids has been limited to 18%[3,6,44], far below the requirements for practical applications. Here, we demonstrate the efficient storage of single photons with the heralding photon at the telecom C-band[45] using the setup illustrated in Fig. 4a. Heralded single-photon generation is achieved via cavity-enhanced non-degenerate spontaneous parametric down-conversion in a periodically poled potassium titanyl phosphate crystal pumped by a 421-nm laser. The poled potassium titanyl phosphate crystal is housed in a symmetric confocal cavity supporting multiwavelength resonance, producing photon pairs at 580 and 1,537 nm. After spectral filtering with interference filters, cascaded etalons and a filter crystal based on an optically pumped 1%-doped Eu^{3+}:Y_2SiO_5 crystal, the final bandwidth of the 580-nm photons is limited to 4 MHz. These telecom-heralded 580-nm single photons are stored in the FBC-based quantum memory. We measure a storage efficiency of 69.8% ± 1.6% at 2 μs (Fig. 4b), setting a new record for the storage efficiency of true single photons in solids, which also significantly outperforms the corresponding efficiency (~33%) of a fibre delay line at the same wavelength. The slight efficiency drop relative to weak coherent inputs arises from the spectrally filtered single-photon wave-packet departing from an ideal Gaussian profile. The second-order cross-correlations between 1,537-nm photons and readout 580-nm photons are measured to be 16.4(2) within a 123-ns window, far exceeding the classical threshold of 2, confirming the non-classical nature of the retrieved signal[44]. With a single-mode duration of 0.5 μs for the heralded single photons, the FBC successfully stored four temporal modes of heralded single photons. Given the C-band heralding photons, this system provides a direct interface for long-distance quantum networks[1,3,45].

Discussion

We have demonstrated integrated quantum memories for light based on both the WGC and the FBC. We achieve multiplexed quantum storage with an efficiency up to 80.3(7)% for weak coherent pulses and 69.8(1.6)% for telecom-heralded single photons. Figure 5 shows an overview of efficient and compact quantum memories implemented across various physical systems. To facilitate a fair comparison of multiplexing capabilities across systems with different storage times, we introduce the effective number of stored modes (N_M), defined as the product of the number of modes and the storage efficiency.

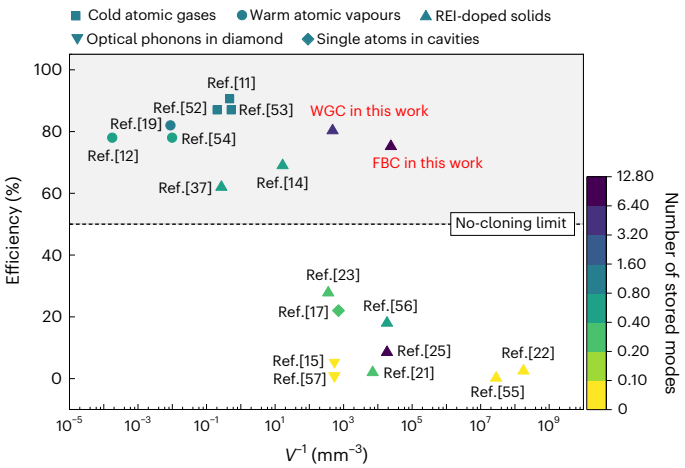

Fig. 5 | Performance overview of quantum memories for light. The horizontal axis represents the inverse of effective volume which corresponds to the number of potential memory units per volume of cubic millimetres. The surveyed physical systems include cold atomic gases[11,52,53], warm atomic vapours[12,19,54], REI-doped solids[14,21–23,25,37,55,56], optical phonons in diamond[15,57] and single atoms in cavities[17], with a focus on those that have demonstrated efficient or small-volume quantum storage. For each experimental work plotted, the reported efficiency corresponds to the maximum measured storage efficiency. The effective volume V of a quantum memory is determined by multiplying the transverse mode area of the optical field with the effective device length (the medium length or the cavity length). The effective number of stored modes (N_M) is calculated as the product of the number of modes and the corresponding storage efficiency, with the colour depth of each data point representing this value.

Using this metric, the FBC and the WGC achieve N_M values of 10.26 and 4.23, respectively. Our work represents the first demonstration of multimode quantum storage with an efficiency surpassing the no-cloning limit of 50% while achieving a device volume as small as 4×10^{-5} mm^3, a reduction of more than three orders of magnitude compared with other efficient quantum memories.

The FBC and the WGC offer complementary strengths in applications. The FBC architecture supports spectrally tunable and efficient quantum storage through variable strain applied to thin membranes, facilitating wideband spectral multiplexing and flexible interfacing with quantum light sources. This tunable quantum memory complements single-atom-based tunable quantum light sources[46,47], forming an efficient interface that could dramatically boost the data rate of multiplexed quantum repeaters[3,45]. Meanwhile, WGCs offer the potential for high-density integration via a three-dimensional femtosecond laser micromachining, enabling spatial multiplexing.

Extending the FBC to long-lived spin-wave storage is straightforward: the planar mirror coating can be engineered for high reflectance at normal incidence but low reflectance at large angles, allowing control pulses to be injected non-collinearly with respect to the signal[48,49]. For the WGC, spin-wave operation can be realized by dual-resonance of two orthogonal polarizations and subsequent polarization-based filtering of the control pulse[50]. The WGC facilitates easy operation at the 'magic' magnetic field, which demands precise tuning of the entire memory device[29,30]. Moreover, fibre pig-tailing and packaging are essential to enhance the practicality of integrated quantum memories. We have previously demonstrated waveguide-based quantum memories with fibre pig-tailing[51]. Extending this capability to WGCs and FBCs introduces additional challenges, with efficient mode matching as a key issue that can potentially be addressed using thermally expanded core fibres or graded-index lenses.

Our results overcome the efficiency barriers of integrated quantum memories and highlight their unique advantages in high-density multiplexing and flexible spectral tunability, clearing the way for their widespread application in large-scale quantum networks and photonic processors.

Online content

Any methods, additional references, Nature Portfolio reporting summaries, source data, extended data, supplementary information, acknowledgements, peer review information; details of author contributions and competing interests; and statements of data and code availability are available at https://doi.org/10.1038/s41566-026-01845-y.

References

1. Sangouard, N., Simon, C., de Riedmatten, H. & Gisin, N. Quantum repeaters based on atomic ensembles and linear optics. *Rev. Mod. Phys.* **83**, 33–80 (2011).
2. Ritter, S. et al. An elementary quantum network of single atoms in optical cavities. *Nature* **484**, 195–200 (2012).
3. Liu, X. et al. Heralded entanglement distribution between two absorptive quantum memories. *Nature* **594**, 41–45 (2021).
4. Kok, P. et al. Linear optical quantum computing with photonic qubits. *Rev. Mod. Phys.* **79**, 135–174 (2007).
5. Nunn, J. et al. Enhancing multiphoton rates with quantum memories. *Phys. Rev. Lett.* **110**, 133601 (2013).
6. Liu, X. et al. Nonlocal photonic quantum gates over 7.0 km. *Nat. Commun.* **15**, 8529 (2024).
7. Zhou, Z.-Q. et al. Photonic integrated quantum memory in rare-earth doped solids. *Laser Photon. Rev.* **17**, 2300257 (2023).
8. Grosshans, F. & Grangier, P. Quantum cloning and teleportation criteria for continuous quantum variables. *Phys. Rev. A* **64**, 010301 (2001).
9. Varnava, M., Browne, D. E. & Rudolph, T. Loss tolerance in one-way quantum computation via counterfactual error correction. *Phys. Rev. Lett.* **97**, 120501 (2006).
10. Julsgaard, B., Sherson, J., Cirac, J. I., Fiurášek, J. & Polzik, E. S. Experimental demonstration of quantum memory for light. *Nature* **432**, 482–486 (2004).
11. Wang, Y. et al. Efficient quantum memory for single-photon polarization qubits. *Nat. Photon.* **13**, 346–351 (2019).
12. Hosseini, M., Campbell, G., Sparkes, B. M., Lam, P. K. & Buchler, B. C. Unconditional room-temperature quantum memory. *Nat. Phys.* **7**, 794–798 (2011).
13. de Riedmatten, H., Afzelius, M., Staudt, M. U., Simon, C. & Gisin, N. A solid-state light–matter interface at the single-photon level. *Nature* **456**, 773–777 (2008).
14. Hedges, M. P., Longdell, J. J., Li, Y. & Sellars, M. J. Efficient quantum memory for light. *Nature* **465**, 1052–1056 (2010).
15. England, D. G., Bustard, P. J., Nunn, J., Lausten, R. & Sussman, B. J. From photons to phonons and back: A thz optical memory in diamond. *Phys. Rev. Lett.* **111**, 243601 (2013).
16. Specht, H. P. et al. A single-atom quantum memory. *Nature* **473**, 190–193 (2011).
17. Körber, M. et al. Decoherence-protected memory for a single-photon qubit. *Nat. Photon.* **12**, 18–21 (2018).
18. Vernaz-Gris, P., Huang, K., Cao, M., Sheremet, A. S. & Laurat, J. Highly-efficient quantum memory for polarization qubits in a spatially-multiplexed cold atomic ensemble. *Nat. Commun.* **9**, 363 (2018).
19. Guo, J. et al. High-performance raman quantum memory with optimal control in room temperature atoms. *Nat. Commun.* **10**, 148 (2019).
20. Nunn, J. et al. Multimode memories in atomic ensembles. *Phys. Rev. Lett.* **101**, 260502 (2008).
21. Saglamyurek, E. et al. Broadband waveguide quantum memory for entangled photons. *Nature* **469**, 512–515 (2011).
22. Zhong, T. et al. Nanophotonic rare-earth quantum memory with optically controlled retrieval. *Science* **357**, 1392–1395 (2017).
23. Liu, C. et al. On-demand quantum storage of photonic qubits in an on-chip waveguide. *Phys. Rev. Lett.* **125**, 260504 (2020).
24. Sinclair, N. et al. Spectral multiplexing for scalable quantum photonics using an atomic frequency comb quantum memory and feed-forward control. *Phys. Rev. Lett.* **113**, 053603 (2014).
25. Seri, A. et al. Quantum storage of frequency-multiplexed heralded single photons. *Phys. Rev. Lett.* **123**, 080502 (2019).
26. Merkel, B., Ulanowski, A. & Reiserer, A. Coherent and Purcell-enhanced emission from erbium dopants in a cryogenic high-Q resonator. *Phys. Rev. X* **10**, 041025 (2020).
27. Casabone, B. et al. Dynamic control of Purcell enhanced emission of erbium ions in nanoparticles. *Nat. Commun.* **12**, 3570 (2021).
28. Meng, R.-R. et al. Solid-state quantum nodes based on color centers and rare-earth ions coupled with fiber fabry–pérot microcavities. *Chip* **3**, 100081 (2024).
29. Zhong, M. et al. Optically addressable nuclear spins in a solid with a six-hour coherence time. *Nature* **517**, 177–180 (2015).
30. Ma, Y., Ma, Y.-Z., Zhou, Z.-Q., Li, C.-F. & Guo, G.-C. One-hour coherent optical storage in an atomic frequency comb memory. *Nat. Commun.* **12**, 2381 (2021).
31. Lau, H.-K., Qiao, H., Clerk, A. A. & Zhong, T. Efficient in situ generation of photon-memory entanglement in a nonlinear cavity. *Phys. Rev. Lett.* **134**, 053602 (2025).
32. Fleischhauer, M., Yelin, S. & Lukin, M. How to trap photons? Storing single-photon quantum states in collective atomic excitations. *Opt. Commun.* **179**, 395–410 (2000).
33. Moiseev, S. A., Andrianov, S. N. & Gubaidullin, F. F. Efficient multimode quantum memory based on photon echo in an optimal QED cavity. *Phys. Rev. A* **82**, 022311 (2010).

34. Afzelius, M. & Simon, C. Impedance-matched cavity quantum memory. *Phys. Rev. A* **82**, 022310 (2010).
35. Sabooni, M., Li, Q., Kröll, S. & Rippe, L. Efficient quantum memory using a weakly absorbing sample. *Phys. Rev. Lett.* **110**, 133604 (2013).
36. Jobez, P. et al. Cavity-enhanced storage in an optical spin-wave memory. *New J. Phys.* **16**, 083005 (2014).
37. Duranti, S. et al. Efficient cavity-assisted storage of photonic qubits in a solid-state quantum memory. *Opt. Express* **32**, 26884–26895 (2024).
38. Sabooni, M., Li, Q., Rippe, L., Mohan, R. K. & Kröll, S. Spectral engineering of slow light, cavity line narrowing, and pulse compression. *Phys. Rev. Lett.* **111**, 183602 (2013).
39. Schraft, D., Hain, M., Lorenz, N. & Halfmann, T. Stopped light at high storage efficiency in a Pr^{3+}:Y_2SiO_5 crystal. *Phys. Rev. Lett.* **116**, 073602 (2016).
40. Horvath, S. P. et al. Noise-free on-demand atomic frequency comb quantum memory. *Phys. Rev. Res.* **3**, 023099 (2021).
41. Galland, N. et al. Mechanical tunability of an ultranarrow spectral feature of a rare-earth-doped crystal via uniaxial stress. *Phys. Rev. Applied* **13**, 044022 (2020).
42. Thorpe, M. J., Rippe, L., Fortier, T. M., Kirchner, M. S. & Rosenband, T. Frequency stabilization to 6×10^{-16} via spectral-hole burning. *Nat. Photon.* **5**, 688–693 (2011).
43. Lago-Rivera, D., Grandi, S., Rakonjac, J. V., Seri, A. & de Riedmatten, H. Telecom-heralded entanglement between multimode solid-state quantum memories. *Nature* **594**, 37–40 (2021).
44. Businger, M. et al. Non-classical correlations over 1250 modes between telecom photons and 979-nm photons stored in $171Yb^{3+}$:Y_2Sio_5. *Nat. Commun.* **13**, 6438 (2022).
45. Zhu, T.-X. et al. A metropolitan-scale multiplexed quantum repeater with bell nonlocality. Preprint at available at https://doi.org/10.48550/arXiv.2508.17940 (2025).
46. Trotta, R. et al. Wavelength-tunable sources of entangled photons interfaced with atomic vapours. *Nat. Commun.* **7**, 10375 (2016).
47. Huang, J.-Y. et al. Stark tuning of telecom single-photon emitters based on a single Er3+. *Chinese Phys. Lett.* **40**, 070301 (2023).
48. Ma, Y.-Z. et al. Elimination of noise in optically rephased photon echoes. *Nat. Commun.* **12**, 4378 (2021).
49. Ortu, A., Holzäpfel, A., Etesse, J. & Afzelius, M. Storage of photonic time-bin qubits for up to 20 ms in a rare-earth doped crystal. *npj Quantum Inf.* **8**, 29 (2022).
50. Liu, Y.-P. et al. A millisecond integrated quantum memory for photonic qubits. *Sci. Adv.* **11**, eadu5264 (2025).
51. Liu, D.-C. et al. On-demand storage of photonic qubits at telecom wavelengths. *Phys. Rev. Lett.* **129**, 210501 (2022).
52. Cao, M., Hoffet, F., Qiu, S., Sheremet, A. S. & Laurat, J. Efficient reversible entanglement transfer between light and quantum memories. *Optica* **7**, 1440–1444 (2020).
53. Cho, Y.-W. et al. Highly efficient optical quantum memory with long coherence time in cold atoms. *Optica* **3**, 100–107 (2016).
54. Ma, L. et al. High-performance cavity-enhanced quantum memory with warm atomic cell. *Nat. Commun.* **13**, 2368 (2022).
55. Craiciu, I. et al. Nanophotonic quantum storage at telecommunication wavelength. *Phys. Rev. Appl.* **12**, 024062 (2019).
56. Rakonjac, J. V. et al. Storage and analysis of light-matter entanglement in a fiber-integrated system. *Sci. Adv.* **8**, eabn3919 (2022).
57. England, D. G. et al. Storage and retrieval of thz-bandwidth single photons using a room-temperature diamond quantum memory. *Phys. Rev. Lett.* **114**, 053602 (2015).

Publisher's note Springer Nature remains neutral with regard to jurisdictional claims in published maps and institutional affiliations.

Springer Nature or its licensor (e.g. a society or other partner) holds exclusive rights to this article under a publishing agreement with the author(s) or other rightsholder(s); author self-archiving of the accepted manuscript version of this article is solely governed by the terms of such publishing agreement and applicable law.

© The Author(s), under exclusive licence to Springer Nature Limited 2026

Methods

WGC configuration

In the WGC configuration (Fig. 1a), the substrate is a $^{151}Eu^{3+}$:Y_2SiO_5 crystal (doping level of 700 ppm) with dimensions 5.0 × 4.0 × 4.9 mm^3 along the crystal's $D_1 \times D_2 \times b$ axes. The $D_1 \times D_2$ facets are polished to form a 12-arcsecond wedge and coated with reflective films, providing reflectivities of $R_1 = 65\%$ and $R_2 = 99.5\%$ at 580 nm, respectively. On-chip electrodes fabricated along the b axis, with 380-μm spacing, enable on-demand retrieval via electric pulse control[23]. Five type IV optical waveguides are fabricated between each pair of electrodes using femtosecond laser micromachining technology. The wedge ensures the cavity resonance of at least one waveguide within the absorption profile of $^{151}Eu^{3+}$. Coating directly on bulk crystals to form a cavity[35] substantially reduces intracavity losses compared with large open cavities[37] but introduces notable spatial mode mismatching. By incorporating optical waveguides, we successfully mitigated this mismatch in the WGC, achieving a mode-matching efficiency of $\eta_M = 98.5\%$, a significant improvement over the 84% mode-matching efficiency reported in ref. 35. After systematic optimization of the fabrication process, the optical waveguide finally achieves ultralow propagation loss of 0.012 (0.1 dB cm^{-1}) (Supplementary Section 3), with an estimated $\epsilon/4\widetilde{d} = 1/28$.

FBC configuration

In the FBC configuration (Fig. 1b), the $^{151}Eu^{3+}$:Y_2SiO_5 membrane, cut from the same crystal boule, has a size of 5 × 4 × 0.2 mm^3 along the $D_1 \times D_2 \times b$ axes. The concave fibre mirror is fabricated using CO_2 laser machining[58]. To minimize intracavity losses, the outer surface of the membrane is directly coated with reflective films, serving as the flat cavity mirror. Reflectivities for the stored light at 580 nm are $R_1 = 96.5\%$ (membrane mirror) and $R_2 = 99.9\%$ (fibre mirror), with an estimated $\epsilon/4\widetilde{d}$ of 1/40. Input light is coupled into the cavity via the membrane flat mirror with $\eta_M = 95(1)\%$. To mitigate cryostat vibration effects on cavity length, passive isolation using springs and active locking with shear piezoelectric actuators are employed. The locked cavity has a length stability below 50 pm, resulting in a storage efficiency loss of less than 0.2% (see Supplementary Section 5 for details).

AFC configuration

Following the absorption-enhanced spectral hole-burning process, the absorption depth d of Eu^{3+} ions in the target band is increased to ~2.6 for the WGC and 0.14 for the FBC. In the AFC preparation process, we prepare AFC with a total bandwidth of 6 MHz, with comb periodicity of 1 MHz and 500 kHz for the WGC and FBC, respectively. To optimize the impedance-matched condition, the finesse of the AFC is adjusted, yielding estimated values of 12 for the WGC and 8 for the FBC. Additional details of the spectral preparation process are provided in the Supplementary Section 2.

Data availability

Data for Figs. 1–5 are available via Figshare at https://doi.org/10.6084/m9.figshare.30987664 (ref. 59). Additional data related to this Article are available from the corresponding authors upon request.

Code availability

The custom codes used to produce the results presented in this Article are available from the corresponding authors upon request.

References

58. Hunger, D. et al. A fiber Fabry–Perot cavity with high finesse. *New J. Phys.* **12**, 065038 (2010).
59. Meng, R.-R. et al. Data for 'Efficient integrated quantum memory for light'. *Figshare* https://doi.org/10.6084/m9.figshare.30987664 (2026).

Acknowledgements

This work is supported by the Quantum Science and Technology-National Science and Technology Major Project (grant no. 2021ZD0301200), the National Natural Science Foundation of China (grant nos. 12222411, 11821404, 12474367 and 12204459) and the Fundamental Research Funds for the Central Universities (grant no. WK2030250135). This work is partially carried out at the USTC Center for Micro and Nanoscale Research and Fabrication. Z.-Q.Z. acknowledges the support from the Youth Innovation Promotion Association CAS.

Author contributions

Z.-Q.Z. designed the experiments and supervised all aspects of this work. M.J., R.-R.M. and X.L. performed the FBC experiments with technical support from Z.-Y.T. and J.-M.C. M.J. locked the cavity for FBC. R.-R.M. realized quantum storage with FBC. X.L. fabricated the device for FBC. P.-X.L. and T.-X.Z. conducted the WGC experiments with assistance from H.-Z.Z. P.-X.L. performed the simulation. T.-X.Z. designed the pumping strategy. P.-J.L. grew the crystal. C.Z. constructed the quantum light source. R.-R.M., P.-X.L., X.L., T.-X.Z., M.J. and Z.-Q.Z. wrote the paper, with input from others. Z.-Q.Z. and C.-F.L. supervised the project. All authors contributed to discussing the experiments and results.

Competing interests

The authors declare no competing interests.

Additional information

Supplementary information The online version contains supplementary material available at https://doi.org/10.1038/s41566-026-01845-y.

Correspondence and requests for materials should be addressed to Ming Jin, Zong-Quan Zhou or Chuan-Feng Li.

Peer review information *Nature Photonics* thanks Erhan Saglamyurek and the other, anonymous, reviewer(s) for their contribution to the peer review of this work.

Reprints and permissions information is available at www.nature.com/reprints.